CrystEngComm

PAPER

View Article Online
View Journal | View Issue

Cite this: *CrystEngComm*, 2014, **16**, 3155

Adsorption and UV/Visible photocatalytic performance of BiOI for methyl orange, Rhodamine B and methylene blue: Ag and Ti-loading effects†

Yohan Park,[a] Yulyi Na,[a] Debabrata Pradhan,[b] Bong-Ki Min[c] and Youngku Sohn*[a]

Received 30th December 2013,
Accepted 17th January 2014

DOI: 10.1039/c3ce42654h

www.rsc.org/crystengcomm

We synthesized echinoid-like BiOI microspheres with various doped concentrations of Ag (0.1, 1.0, 5.0, 10.0 mol%) and Ti (1.0, 5.0, 10.0, 30.0, 50.0 mol%) in ethylene glycol and then examined their fundamental properties by scanning electron microscopy, transmission electron microscopy, X-ray diffraction analysis, UV-visible absorption, FT-IR, Raman, photoluminescence and Brunauer–Emmett–Teller (BET) surface area measurements. We also measured the adsorption and photocatalytic dye-degradation performance of the catalysts using methyl orange (MO), Rhodamine B (RhB) and methylene blue (MB). The adsorption performance was found to be in the order of MO < RhB < MB, and to depend somewhat upon the Ag and Ti-loadings. MO was degraded in the order of BiOI < Ag–BiOI < Ti–BiOI under UV and visible light irradiation, while the degradation of RhB was in the order of Ag–BiOI ≈ Ti–BiOI ≪ BiOI, and Ag–BiOI < BiOI < Ti–BiOI, respectively. MB showed poor photodegradation under UV and visible light. Finally, we used an indirect chemical probe method with active species scavengers and photoluminescence spectroscopy to clarify the dye-sensitized photodegradation mechanism. In the mechanism, $^{\bullet}O_2^-$ and h^+ were active species under visible light irradiation. No $^{\bullet}OH$ radicals were found by luminescence spectroscopy.

1. Introduction

Water treatments and impurity removal aided by adsorption and photocatalysis using a catalyst are very important. Bismuth oxyhalides (BiOX, X = Cl, Br and I) have recently been extensively investigated for use as adsorbents and photocatalysts for the removal of unwanted pollutants.[1–47] Since the adsorption and photocatalytic performance are commonly determined by morphology (*e.g.*, sizes and crystal facets) and composition, many studies have been conducted to tailor the morphology and synthesize hybrid materials. Two morphologies of 3D-echinoid-like (or 3D-hierarchical flower-like) and 2D-sheets (or 2D-plates) have commonly been obtained and reported for BiOX. In many tested systems such as those that evaluate dye removal, the 3D BiOX structure has shown much higher adsorption and photocatalytic activities than the 2D structure.[35]

Recently, more extensive research has focused on designing hybrid materials with BiOI to further enhance the catalytic activity under visible light irradiation. The reported hybrid materials include AgI/BiOI[1,2,4,47] Ag/AgI/BiOI,[10,11] Ag/BiOI,[29,30] TiO_2/BiOI,[31,35,36] MnO_x–BiOI,[3] BiOI/ZnSn(OH)$_6$,[5] BiOI/Bi_2WO_6,[6,7] BiOI/$BiPO_4$,[13] Ag_3PO_4/BiOI,[18] Bi/BiOI,[19] BiOI–MWCNT,[21] BiOI/*n*-$ZnTiO_3$[20] BiOI/BiOX,[22,24,26,37,41,42] Bi_2S_3/BiOI,[27] $Bi_2O_2CO_3$/BiOI,[28] BiOI/B_2O_3,[38,39] ZnO/BiOI,[40] and Pt/BiOI.[46] The heterojunction material commonly enhances visible light absorption and further facilitates good electron–hole transport and separation, which results in the effective removal of impurities by photoabsorption. When an n-type (*e.g.*, ZnO and TiO_2) material with a higher band gap (3.0–4.0 eV) is junctioned with p-type BiOI with a lower band gap of ~1.8 eV, visible light irradiation creates an electron and a hole in the conduction and valence bands in BiOI, respectively.[35,36,40] The electrons are then efficiently transferred to the conduction band of the p-type material, leaving the hole in the valence band of BiOI. This process facilitates the electron–hole pair separation without recombination. Metallic nanoparticles such as Ag have been reported to facilitate the capture of photogenerated electrons by surface oxygen to form superoxide ($^{\bullet}O_2^-$) radicals, which act as oxidants[30] Cheng *et al.* demonstrated that AgI/BiOI hierarchical hybrids show much higher photocatalytic 2,4-dichlorophenol decomposition than unhybridized BiOI, and the activity was shown to

[a] *Department of Chemistry, Yeungnam University, Gyeongsan 712-749, Republic of Korea. E-mail: youngkusohn@ynu.ac.kr; Fax: +82 53 810 4613; Tel: +82 53 810 2354*
[b] *Materials Science Centre, Indian Institute of Technology, Kharagpur 721 302, W.B., India*
[c] *Instrumental Analysis Center, Yeungnam University, Gyeongsan 712-749, Republic of Korea*

† Electronic supplementary information (ESI) available. See DOI: 10.1039/c3ce42654h

decrease with the decreasing Ag nanoparticle size.[1] It has been reported that photoinduced holes in the AgI/BiOI hybrid materials are the main factor responsible for the degradation of organic pollutants.[47] Major active intermediate species include hydroxyl radicals ($^{\bullet}OH$), superoxide radicals ($^{\bullet}O_2^-$), electrons (e^-) and holes (h^+). DMPO (5,5-dimethyl-1-pyrroline N-oxide) EPR (electron paramagnetic resonance) spin trapping techniques have been employed to detect these species.[48,49] LC-MS (liquid chromatography-mass spectrometry)[19] and LC-SIR (selected ion recording)-MS were employed to detect the intermediates of the photocatalytic reactions for tetrabromobisphenol[50] and carbamazepine.[51] As an indirect chemical probe method, scavengers of the active species were added during the photoreaction,[22,27,49] after which the dye degradation rate was measured.

Ideally, a catalyst should be multifuncational under any environmental conditions. In the present study, we examined the adsorption and photocatalytic performance of hierarchical echinoid-like (or flower-like) BiOI with different doped concentrations of Ag and Ti for the degradation of methyl orange (MO), Rhodamine B (RhB) and methylene blue (MB), which have different molecular structures and UV-visible absorption bands. We chose two different (Ag and Ti-loaded) catalytic systems for comparison. Ag was chosen because the Ag^+ ion reacts with I^- of BiOI to form AgI with a band gap of ~2.8 eV[47] higher than that (~1.8 eV) of BiOI. On the other hand, Ti does not chemically react with BiOI, and TiO_2 is the most well known photocatalyst with a band gap of 3.2 eV.[16] It was reported that a higher band gap material can be combined with the lower band gap material BiOI to obtain a synergic photocatalytic effect.[1,2,4,10,11,29–31,35,36,47] The originality of this work is further discussed later. The results presented herein provide a clearer understanding of hybrid BiOI adsorption and degradation mechanisms and therefore a deeper scientific insight that will be useful for the development of catalysts/adsorbents for use in water treatment facilities and environmental remediation projects.

2. Experimental section

2.1. Catalyst preparation

Echinoid-like BiOI nanostructures were synthesized as follows. Stoichiometric amounts of $Bi(NO_3)_3{\cdot}5H_2O$ (98%, Junsei, Japan) and KI (99.5%, Samchun Pure Chem., Korea) were completely dissolved in 20 mL ethylene glycol (99.5%, Samchun Pure Chem., Korea), after which the transparent yellow solution was transferred to a Teflon bottle that was tightly capped and placed in an oven (120 °C) for 12 hours. The final reddish-color products were fully washed with Millipore water and ethanol repeatedly, after which they were dried in an oven (80 °C) for 24 hours. We added appropriate amounts of a 0.1 M silver nitrate solution (Yakuri, Japan) or titanium(IV) isopropoxide (98%, Junsei, Japan) to dope the samples with Ag (0.1, 1.0 5.0 and 10.0 mol%) and Ti (1.0, 5.0, 10.0, 30.0 and 50.0 mol%), respectively, before adding KI, after which we followed the same procedures described above.

2.2. Catalyst characterization

The surface morphology of the powder samples was observed by scanning electron microscopy (SEM, Hitachi SE-4800). The microstructures of the catalyst powder were examined by transmission electron microscopy (TEM) and high resolution TEM (HRTEM) using a Tecnai F20 G2 FEI-TEM operated at 200.0 kV. The structural property of samples was further obtained from the electron diffraction patterns. The energy-dispersive X-ray spectroscopy (EDX) measurement was carried out to check the elemental composition of the samples. Additionally, the powder X-ray diffraction (XRD) patterns were evaluated using a PANalytical X'Pert Pro MPD diffractometer with Cu Kα radiation (40 kV and 30 mA). The UV-visible absorption spectra of the powder samples were obtained using a Varian Cary 5000 UV-visible-near IR (UV-Vis-NIR) spectrophotometer (Agilent Technologies). The Fourier-transform infrared (FT-IR) spectra were acquired using a Thermo Scientific Nicolet iS5 spectrometer. The Raman spectra of the pelletized samples were recorded using a Bruker Senterra Raman spectrometer with a laser excitation energy of 758 nm. The photoluminescence spectra were collected using a SCINCO FluoroMate FS-2 at excitation wavelengths of 250 and 280 nm with a Xe lamp source. The Brunauer–Emmett–Teller (BET) surface area was measured using a Quantachrome ChemBET TPR/TPD analyzer with a thermal conductivity detector and 30% N_2/He.

2.3. Catalyst performance tests

To test the adsorption performance of the catalysts, we dispersed 10 mg of a sample into 50 mL of a dye (MO, RhB and MB at 5 mg L^{-1}) solution and then measured the change in the concentration of the dye solution with time under dark conditions. Specifically, the concentration was measured based on the UV-visible absorption intensity using a Jasco V-530 UV-Vis absorption spectrophotometer. For the photocatalytic dye degradation experiments, we dispersed 10 mg of BiOI, 5 mol% Ag–BiOI, or 10 mol% Ti–BiOI catalysts in a dye (MO, RhB and MB) solution (10 mg L^{-1}, 50 mL). Following the adsorption of the dye for 2 hours under dark conditions, we irradiated the samples with visible (using a halogen lamp) or UV (using an UV lamp irradiating 352 nm) light. After selected irradiation times, we measured the concentration of the dye solution using a UV-visible absorption spectrophotometer (Jasco V-530). An indirect scavenger method was employed to examine the roles of the active species such as $^{\bullet}OH$, $^{\bullet}O_2^-$ and h^+, with isopropyl alcohol (IPA), benzoquinone (BQ) and EDTA used as scavengers for $^{\bullet}OH$, $^{\bullet}O_2^-$ and h^+, respectively.[22,27,41,49] Following irradiation with visible ($\lambda > 420$ nm) light, we measured the UV-visible absorption of the dye solutions containing the scavenger. Photoluminescence was employed to detect active $^{\bullet}OH$ radicals using a terephthalic acid solution with the catalyst after visible light irradiation.[26]

3. Results and discussion

3.1. Morphology, crystal structure and growth mechanism

Fig. 1 and 2 show the SEM images of the undoped, Ag-loaded (0.1, 1, 5 and 10 mol%) and Ti-loaded (1, 5, 10, 30 and 50 mol%) BiOI prepared in ethylene glycol, respectively. The SEM image of the undoped BiOI shows an echinoid-like microsphere structure with a size of about 1–2 μm and a surface that appears like a connection of vertically staked walls. When 0.1 mol% Ag was loaded into the BiOI, the morphology showed no critical change. However, when 1.0 mol% Ag was loaded into the BiOI, the surface changed significantly. Specifically, as the Ag-loading increased, the size of the microspheres became smaller and distorted. In addition, many small clusters were shown on the surface. This change in the morphology is very similar to that of the AgI/BiOI hierarchical hybrid structures reported by Cheng *et al.*[1] The observation of the SEM images of the Ti-loaded samples revealed a little change with increasing the Ti-loading amount compared to the Ag-loaded samples. As the Ti-loading increased, the surface showed a wave-like structure and the sphere size became smaller.

As shown in Fig. 3, the 3D-hierarchical echinoid (or flower)-like microspheres appear to be formed by a 3D-assembly growth mechanism. In this process, small BiOI crystal units (with Ag and Ti units) are formed by a reaction of $Bi^{3+} + I^- + H_2O \rightarrow BiOI + 2H^+$. These small units initially grow into sheets that subsequently dissolve and re-grow on larger particles by making connections between vertically stacked sheets *via* the Ostwald ripening process.[25,52,53] The 3D-self-assembly process minimizes the surface energy required to consequently form the microspheres. The Ag or Ti units are embedded inside the 3D structure during crystal growth.

We further examined the microstructures of the catalysts using TEM and HRTEM. Fig. 4 displays the TEM, HRTEM and HAADF images and the selected area electron diffraction (SAED) patterns of the BiOI, Ag–BiOI (10 mol%) and Ti–BiOI (50 mol%) samples. The HRTEM image of BiOI showed clear lattice fringes with a spacing of 0.303 nm, corresponding to

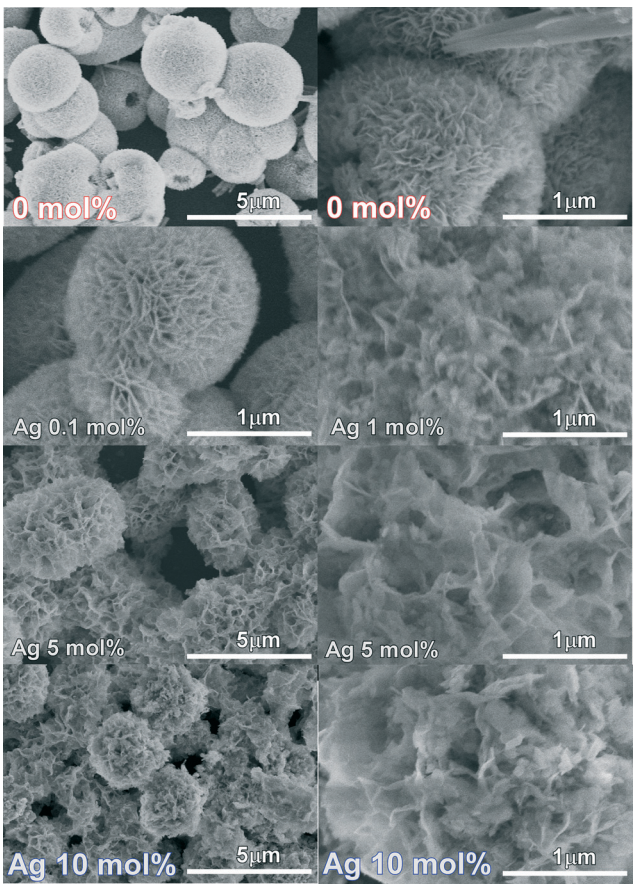

Fig. 1 SEM images of BiOI doped with different concentrations (0.1, 1, 5 and 10 mol%) of Ag.

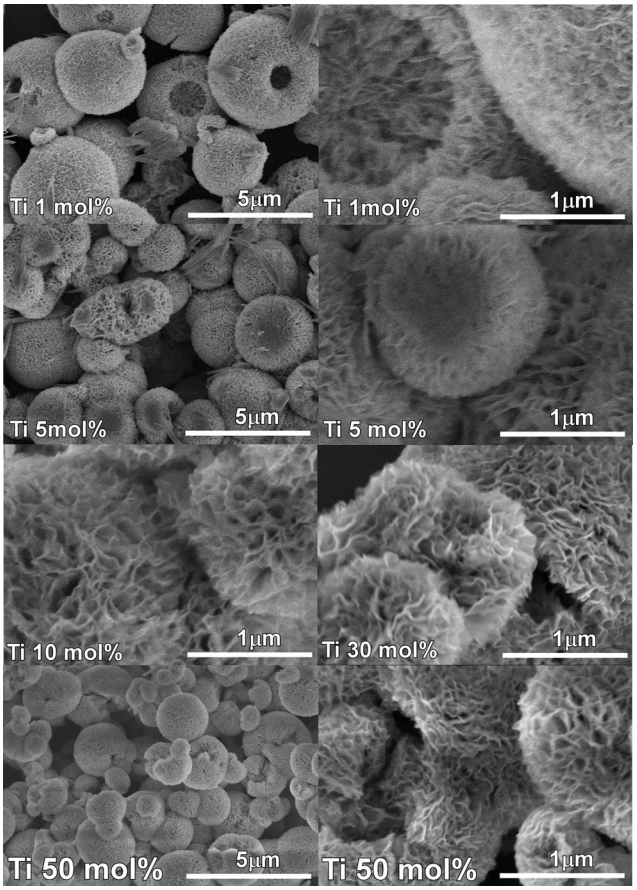

Fig. 2 SEM images of BiOI doped with different concentrations (1, 5, 10, 30 and 50 mol%) of Ti.

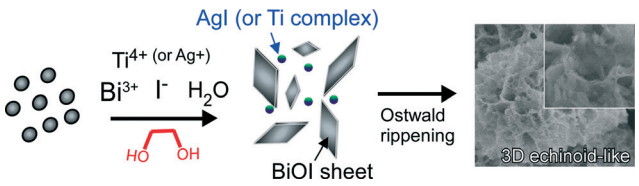

Fig. 3 A plausible growth mechanism of the echinoid-like Ag and Ti-loaded BiOI nanostructures.

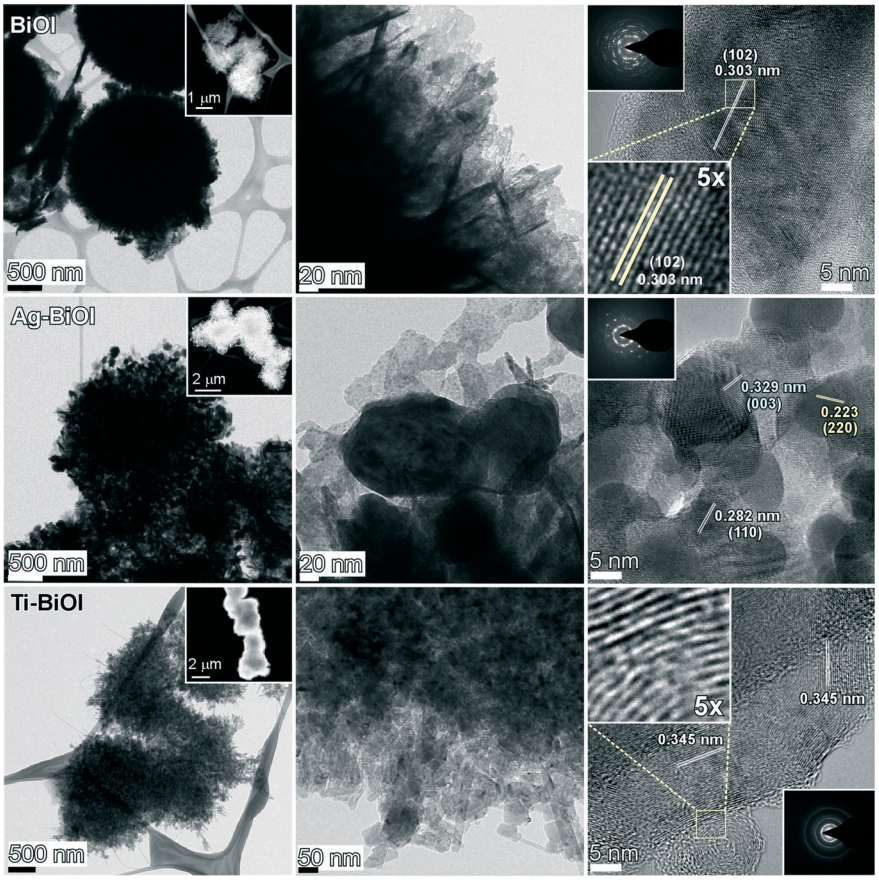

Fig. 4 TEM (left and middle columns), HRTEM (right column) and high-angle annular dark field (HAADF) TEM images (inset, left column) of the BiOI, Ag–BiOI (10 mol%) and Ti–BiOI (50 mol%) samples. The insets (right column) show the corresponding electron diffraction patterns.

the {102} facet of tetragonal BiOI. The SAED pattern also indicates the crystalline nature of the sample. For Ag–BiOI, small clusters appear to be embedded in the microstructure as shown in the TEM image. The surface area may be decreased due to the formation of the clusters, which is discussed later. The HRTEM image shows the various lattice fringes with spacings of 0.282 nm, 0.329 nm and 0.223 nm. These correspond to the {110} facet of BiOI, the {003} facet of BiO and the {220} facet of AgI, respectively. For the HRTEM image of Ti–BiOI (50 mol%), interestingly the lattice spacing became wider with 0.345 nm, and the planes show a staked structure. It appears that during the crystal growth, titanium(IV) isopropoxide may incorporate between the BiOI layers to expand the lattice spacing. Furthermore, the ring SAED suggests the polycrystalline nature of the sample as confirmed from the broad XRD feature (discussed later). Since the size of the Ti atom is smaller than that of the Bi atom, Ti may easily incorporate into the BiOI lattice.[54] Li *et al.* synthesized BiOBr–Bi_2WO_6 mesoporous nanosheet composites with and without titanium(IV) isopropoxide.[55] They found that titanium(IV) isopropoxide induces pores in the nanosheets and impacts on the facet formation.

Fig. 5 displays the powder XRD patterns of undoped, Ag-loaded (0.1, 1, 5 and 10 mol%) and Ti-loaded (1, 5, 10, 30 and 50 mol%) BiOI prepared in ethylene glycol. The XRD patterns of the undoped flower (or echinoid)-like 3D-BiOI matched those of tetragonal (*P*4/*nmm*) BiOI (JCPDS 10-0445) well.[32,34,35,39] The four major peaks at 2θ = 29.3°, 31.8°, 45.6° and 55.1° were assigned to the (102), (110), (200) and (212) planes, respectively.[34,35,39] Other minor peaks were also assigned to the corresponding XRD peaks. As the Ag-loading increased, new XRD peaks appeared, although the XRD peaks of BiOI were still predominant. The new patterns of the 10 mol% Ag-loaded BiOI matched those of hexagonal (*P*63*mc*) AgI (JCPDS 9-0374). In addition to the XRD peaks of AgI, a shoulder near the (102) peak was found, which was tentatively attributed to rhombohedral (JCPDS 1-075-0995) bismuth oxide (BiO). During the precipitation and crystal growth process, Ag^+ reacts with I^- to form AgI[1,2,4,10,11] *via* an ion exchange process (*e.g.*, $BiOI + Ag^+ \rightarrow AgI + BiO^+$). During this process, AgI is embedded in the 3D-BiOI structure. For the Ti-loaded BiOI, the XRD peak positions were very similar; however, as shown in the inset of Fig. 5, some XRD peaks became much broader than others. No XRD peak of TiO_2 was observed. The (102) peak of BiOI was significantly broadened with the increasing Ti amount, and the (110) peak was shifted to a larger 2θ angle. This is possibly due to the facets affected by Ti and the incorporation of Ti into the BiOI lattice during the crystal growth. Although, no XRD peaks were obtained from TiO_2 embedded in the lattice, the EDX

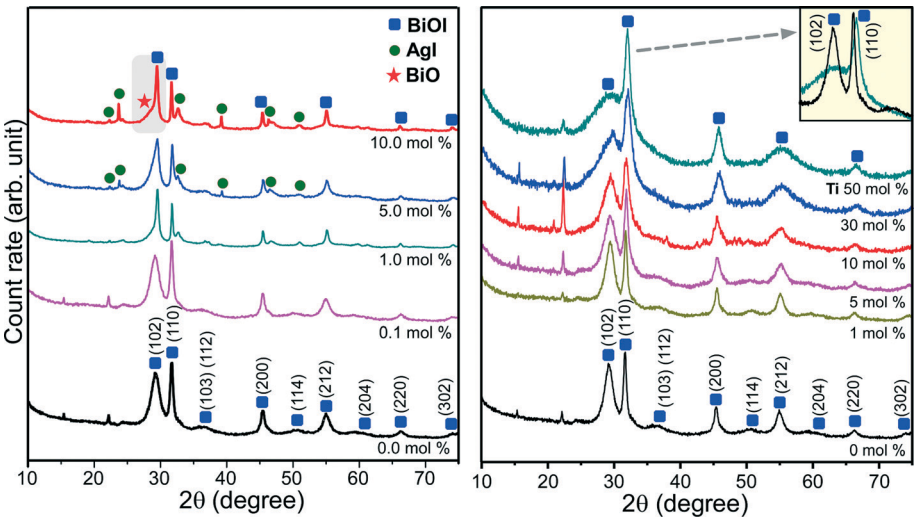

Fig. 5 The power X-ray diffraction patterns of BiOI with increasing Ag (left) and Ti (right) loadings. The inset (right) shows the difference in the (102) and (110) peaks between undoped BiOI and 10 mol% Ti–BiOI.

measurement confirms the presence of Ti (Fig. S1, ESI†). This suggests that the Ti is embedded in the lattice of BiOI as an amorphous form. Wei *et al.* prepared BiOBr–TiO_2 catalysts using tetra-butyl titanate.[54] They also did not observe XRD peaks of crystalline Ti-species, and attributed the Ti to the amorphous phase.

3.2. Band gaps, Raman spectra and photoluminescence

The UV-Vis reflectance absorption spectra of the Ag-loaded (0.1, 1, 5 and 10 mol%) and Ti-loaded (1, 5, 10, 30 and 50 mol%) BiOI are displayed in Fig. 6. The absorbance *Y*-axis data were converted from diffuse reflectance data by the Kubelka–Munk method. For the Ag-loaded samples, the absorption edge showed no critical change as the Ag amount was changed, which is in good agreement with the results reported by Lv *et al.*[4] However, the edge of the Ti-loaded sample shifted to a shorter wavelength when the Ti amount was increased. The brown color of the Ag-loaded samples remained about the same while the Ti-loaded sample became white-brown when the Ti amount was increased. The optical band gaps were estimated using the Tauc equation, $\alpha h\nu = A(h\nu - E_g)^{n/2}$, where A is an empirical constant, and $n = 1$ for the direct band gap and $n = 4$ for the indirect band gap.[2,4,9,20,56] The indirect band gaps were obtained from the intersection of the plot of $[\alpha h\nu]^{1/2}$ *versus* $h\nu$. For undoped BiOI, the indirect band gap was estimated to be 1.82 eV, and this value showed a small change upon the Ag loading to 1.83 eV for the 10 mol% Ag-loaded BiOI. For the Ti-loaded sample, the band gap became gradually increased when the Ti amount was increased to 1.92 eV for the 50 mol% Ti-loaded BiOI. Xia *et al.* reported a band gap of 1.84 eV for the flower-like porous BiOI microspheres,[57] which is in good agreement with the results of the present study. A band gap of 1.76 eV for sheet-shaped single-crystalline BiOI was reported by Chang *et al.*[56] Band gap energies of 1.77 and 1.72 eV were reported for BiOI nanoflakes and nanoplates, respectively.[44] However, a much lower band gap of 1.46–1.63 eV was reported for BiOI prepared using a microwave irradiation in a mannitol solution.[17]

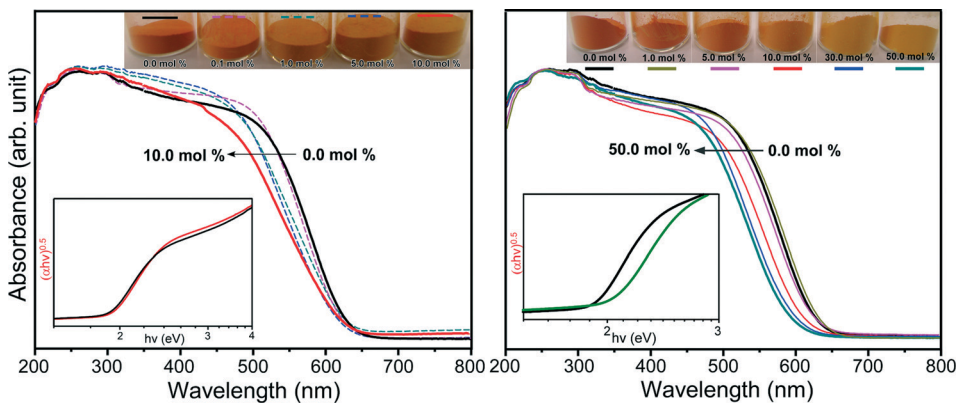

Fig. 6 The UV-Visible diffuse reflectance absorption spectra of BiOI with increasing Ag (left) and Ti (right) loadings. The insets (top) show the photographs of the corresponding samples. The lower left insets show the plots of $[\alpha h\nu]^{1/2}$ *versus* $h\nu$ for BiOI, 10 mol% Ag–BiOI and 50 mol% Ti–BiOI.

Fig. 7 displays the Raman spectra of BiOI doped with different concentrations of Ag and Ti. The corresponding FT-IR spectra are provided in Fig. S2, ESI.† A peak at 148 cm^{-1} attributed to the E_g mode (internal Bi–I stretching) was found in all of the Raman spectra, which is in good agreement with previous studies.[24,27] The B_{1g} and A_{1g} modes were nearly absent. The vibrational modes of BiOI with a tetragonal structure ($P4/mmm$) are represented as $\Gamma = 2A_{1g} + B_{1g} + 3E_g + 2E_u + 2A_{2u}$, where A_{1g}, B_{1g} and $3E_g$ are Raman active, and the others are IR active.[2,12,22,24] The major peak position showed no critical change as the amounts of Ag and Ti changed, indicating that the major BiOI structure was preserved regardless of the guests, which agrees well with the XRD results (Fig. 5).

Fig. 8 displays the photoluminescence (PL) spectra of the BiOI, Ag and Ti-loaded BiOI catalysts at an excitation wavelength of 280 nm. A broad peak was commonly observed at around 600 nm.[32,46] Yu *et al.* also observed a broad peak at ~600 nm for the BiOI nanoplates.[46] Photoluminescence (PL) spectroscopy has commonly been employed to predict the photocatalytic efficiency of a catalyst. Since the electrons and holes play major roles in the photocatalytic reaction the catalytic activity decreases when an electron and a hole recombine to emit a photon.[2,20,58] For this reason, catalysts with a high PL will generally have a lower photocatalytic performance. The PL intensity of BiOI increased by about the same amount upon the Ag and Ti-loadings. Based on the PL data alone, the photocatalytic activity of the Ag and Ti-loaded BiOI should be lower; however, the observed photocatalytic activity was not consistent with the PL results, indicating that other factors are also involved in the photocatalytic mechanism.

3.3. The adsorption of MO, RhB and MB, and the BET surface area

We tested the adsorption performance of BiOI, Ag-doped BiOI and Ti-doped BiOI using methyl orange (MO), Rhodamine B (RhB) and methylene blue (MB) under dark conditions after just 10 min (Fig. 9). For undoped BiOI, about 10% of MO and 90% of RhB and MB were adsorbed, which suggests that BiOI is not a suitable catalyst for MO adsorption. For 0.1 mol% Ag-doped BiOI, the adsorption performance was slightly enhanced, compared with BiOI. The adsorption performance became poor when the Ag-loading was increased above 1 mol% for all of the dyes *i.e.* MO, RhB and MB (left side, Fig. 9). For the Ti-loaded BiOI with MO (top right, Fig. 9), the adsorption performance was increased with increasing Ti-loading up to 30 mol%. The 0.1 mol% Ag

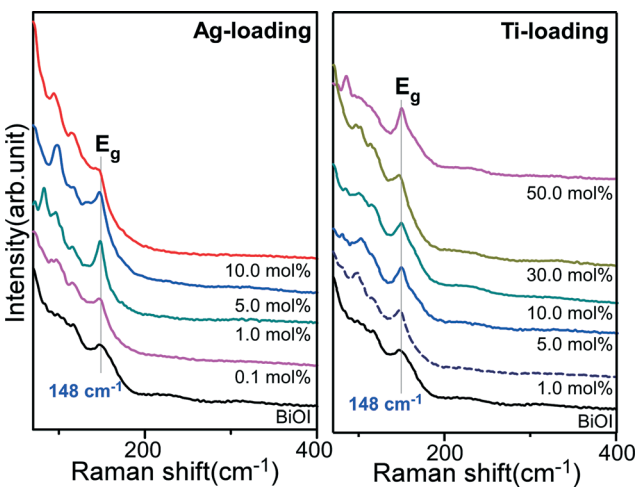

Fig. 7 The Raman spectra of BiOI with increasing Ag (left) and Ti (right) loadings.

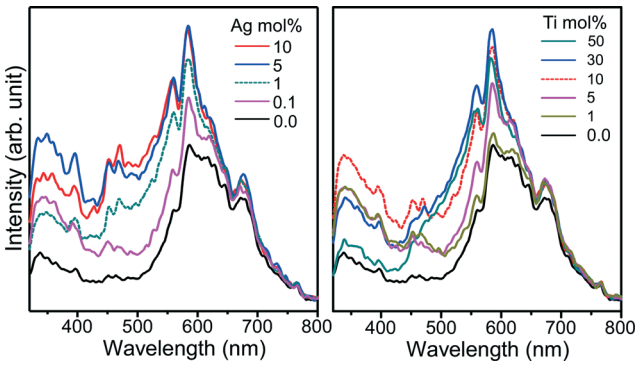

Fig. 8 The photoluminescence spectra of BiOI with increasing Ag (left) and Ti (right) loadings at an excitation wavelength of 280 nm.

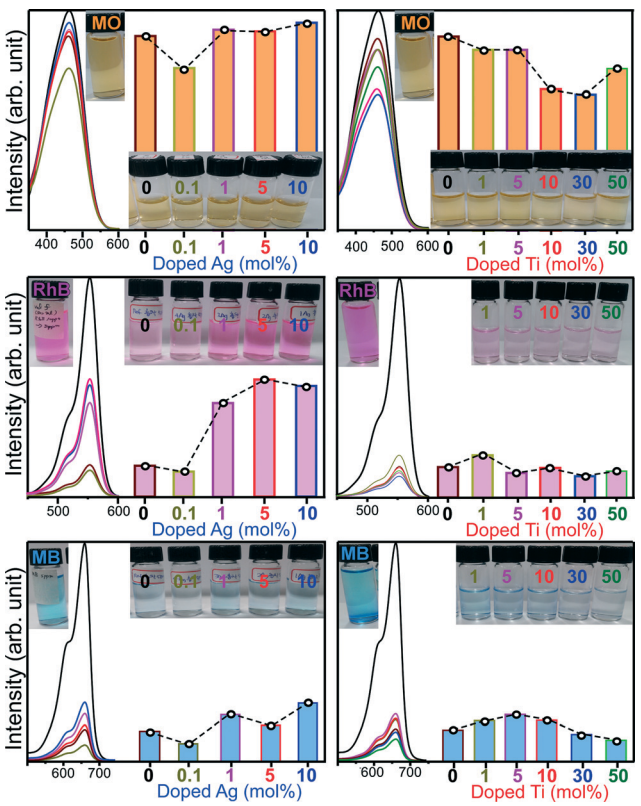

Fig. 9 The UV-visible absorption spectra and the corresponding peak intensities upon the adsorption of MO, RhB and MB (5 mg L^{-1}, 50 mL) by 10 mg BiOI, Ag-doped BiOI and Ti-doped BiOI. The insets show the photo images of the corresponding dye solutions after adsorption. All the absorption peaks were normalized before adsorption.

doped BiOI showed the highest adsorption of RhB (middle left, Fig. 9). For RhB, the adsorption performance of Ti-loaded BiOI was found to be almost the same except for 1.0 mol% Ti–BiOI (middle right, Fig. 9). For the MB dye, the adsorption performance was lower with 1, 5, and 10 mol% Ti–BiOI, but higher with 30 and 50 mol% Ti–BiOI. Among these dyes, the adsorption was commonly found to be in the order of MO $\ll$ RhB $<$ MB, which is in good agreement with the literature.[59] Zhang *et al.* reported that the BiOBr catalysts showed a better absorption performance for RhB and MB than for MO,[59] which is consistent with the results of the present study. They attributed the higher adsorption ability of RhB and MB to stronger electrostatic interactions between the dyes and the BiOBr surface. Similarly, because RhB and MB are positively charged while MO is negatively charged in solution, the negatively surface charged BiOI will interact more strongly with RhB and MB.

Since the surface area of a catalyst is related to the adsorption, the BET surface areas (Fig. S3, ESI†) were measured. These values are summarized in Tables 1 and 2 for the Ag and Ti-loaded BiOI catalysts, respectively. Before loading Ag and Ti, the 3D-flower like BiOI exhibited a BET surface area of 60.8 m^2 g^{-1}, which is larger than the values reported in previously conducted studies.[3–5,13,20,27,41,57] Xia *et al.* measured BET specific surface areas of 28.3 m^2 g^{-1} and 5.3 m^2 g^{-1} for 3D flower-like BiOI and 2D-plates, respectively.[57] Upon loading 0.1% Ag into BiOI, the surface area increased slightly, while loading more than 1 mol% led to a significant decrease in the BET area. For the Ti-loading below 10 mol%, the surface areas were similar compared with that of undoped BiOI, while the 30 and 50 mol%-Ti samples showed a dramatic increase in the BET surface area. Overall, for the higher loading of Ag (1, 5 and 10 mol%) and Ti (30 and 50 mol%), the BET surface area was correlated with the adsorption performance. In other words, the surface area effect was more dominant than other effects. For the lower Ag and Ti loadings, the adsorption of a dye onto the catalyst was more likely dependent on the nature (*e.g.*, surface charge and molecular dipoles) of the dye and the catalyst.[59]

3.4. The photocatalytic performance of MO, RhB and MB under UV and visible light

Prior to examining the detail photocatalytic performance we selected 5 mol% Ag– and 10 mol% Ti–BiOI as representative test materials based on the XRD and adsorption data. The 5 mol% Ag– and 10 mol% Ti–BiOI were enough to show differences in the XRD and adsorption performance, compared with those of un-loaded BiOI. For the selected three catalysts, we tested the adsorption of MO, RhB and MB with a dye concentration of 10 mg L^{-1} under dark conditions (Fig. S4, ESI†). Upon adsorption, we examined the photodegradation of MO, RhB and MB by the three (BiOI, 5 mol% Ag–BiOI and 10 mol% Ti BiOI) selected catalysts under UV ($\lambda < 420$ nm) and visible ($\lambda > 420$ nm) light irradiation (Fig. 10).[60] Without the catalyst, we observed no significant degradation of the dye under UV or visible light irradiation, indicating that a charge transfer process between the dye and the catalyst may be an important factor for improving dye degradation (discussed in detail below). After the adsorption of the three different dyes for 2 hours in the dark, we started irradiation with UV or visible light.

Fig. 10 displays the photodegradation rates (change in peak position and UV-visible absorption spectra) of the MO, RhB and MB solutions with BiOI, 5 mol% Ag-loaded BiOI and 10 mol% Ti-loaded BiOI under UV and visible light irradiation. For MO, the degradation rate (or the change in peak position) was very similar under UV and visible irradiation. Specifically, the degradation performance showed the order of BiOI $<$ Ag–BiOI $<$ Ti–BiOI, and the Ti-loaded BiOI showed the best photocatalytic performance for MO dye. For RhB, the photocatalytic activity differed greatly under UV and visible irradiation. Specifically, RhB with BiOI was efficiently degraded with time under UV irradiation, while RhB with the Ag and Ti-loaded BiOI catalysts showed very little degradation with time. The doped catalysts showed a very poor photocatalytic activity for RhB under UV irradiation. However, under visible light irradiation the Ag and Ti-doped catalysts showed a good photocatalytic activity comparable to or better than that of undoped BiOI. Overall, the catalytic activity was in the order of Ag–BiOI $<$ BiOI $<$ Ti–BiOI. Ti-loaded BiOI showed a very good photocatalytic activity toward RhB under visible light irradiation, implying that the dye degradation occurs *via* a dye sensitized mechanism,[61,62] as discussed in detail below. In addition, the different exposed facets showed different reactivities between UV and visible light.[45] Although MB was the most efficiently adsorbed onto the catalyst surface, it was not efficiently photodegraded under UV and visible light irradiation. The peak position showed no change with time. The concentration of the MB solution showed no linear decrease with irradiation time (UV and visible) when treated with the BiOI and Ag and Ti-loaded BiOI catalysts (Fig. S5, ESI†), suggesting that the MB dye could be removed efficiently by adsorption, but not by photocatalytic reaction. The photocatalytic performance has been shown to be more closely related to the exposed facets of a catalyst than the surface area.[43,45,63] In the dye-sensitized mechanism, a good charge

Table 1 The BET surface areas (m^2 g^{-1}) of reference (undoped) BiOI and Ag-doped BiOI with different Ag concentrations

Ag mol%	0	0.1	1	5	10
Surface area (m^2 g^{-1})	60.8	66.2	44.3	45.1	44.2

Table 2 The BET surface areas (m^2 g^{-1}) of reference (undoped) BiOI and Ti-doped BiOI with different Ti concentrations

Ti mol%	0	1	5	10	30	50
Surface area (m^2 g^{-1})	60.8	57.8	70.5	58.0	98.8	111.5

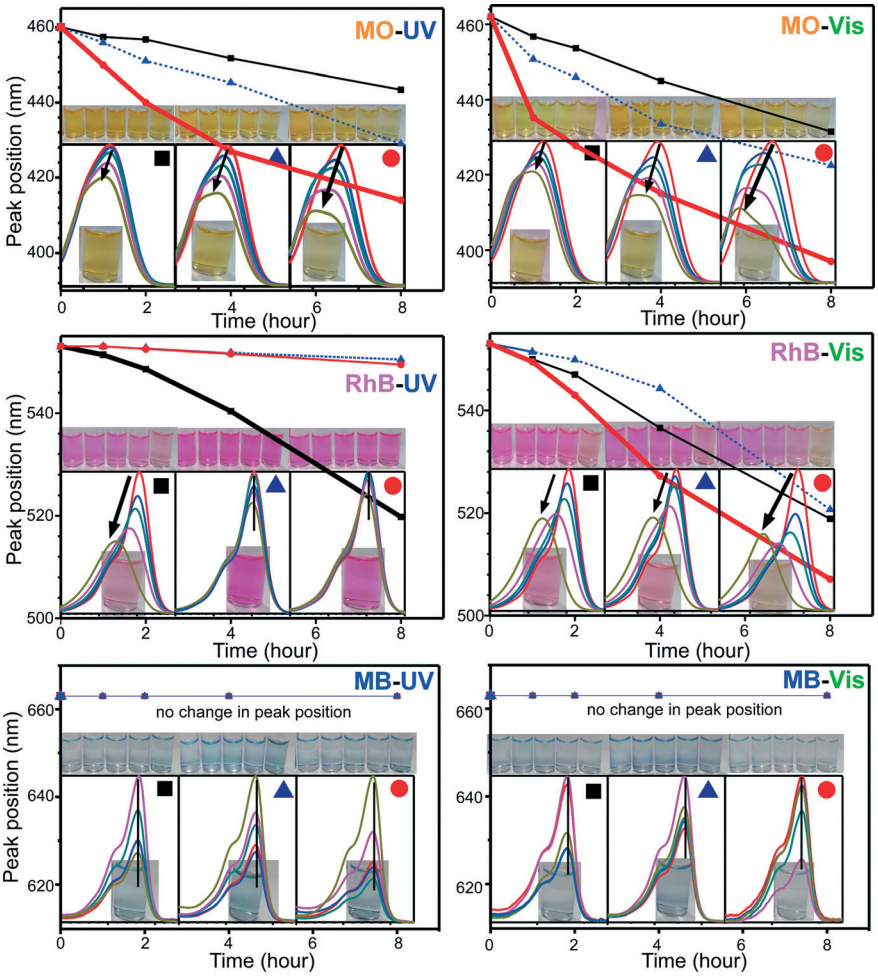

Fig. 10 Photodegradation (change in peak position and UV-visible absorption spectra) of the MO, RhB and MB solutions (10 mg L^{-1}, 50 mL) by BiOI (■), 5 mol% Ag-loaded BiOI (▲) and 10 mol% Ti-loaded BiOI (●) under UV (left column) and visible (right column) light irradiation. The insets show the photos of the corresponding solutions with photodegradation time. The absorption wavelengths of the dyes (Fig. S6, ESI†) were omitted for clarity.

transfer followed by separation is an important step, and is mainly determined by the exposed facet. The LUMO of a dye and the CB of a catalyst is another important factor for the higher charge transfer. A good interfacial wavefunction mixing (or a well-aligned energy level) promotes the charge transfer rate.

To clearly examine the photocatalytic mechanism and the role of the active species, we employed an indirect chemical probe method using scavengers of isopropyl alcohol (IPA), benzoquinone (BQ) and EDTA for the $^{\bullet}OH$, $^{\bullet}O_2^-$ and h^+ species, respectively. Fig. 11 displays the photocatalytic degradation of RhB for BiOI, Ag(5 mol%)–BiOI and Ti(50 mol%)–BiOI in the absence and presence of scavengers (IPA, BQ and EDTA) under visible ($\lambda > 420$ nm) light irradiation for 6 hours. It should be noted that the photocatalytic activity is dependent on the amount of Ag and Ti-loading. Jiang *et al.* prepared Ag and Ti-decorated flower-like BiOBr microspheres and found that the photocatalytic activity was highly dependent on the Ag or Ti-content.[64] The dye without a scavenger showed the greatest degradation (or the shift in peak position), with an order of Ag(5 mol%)–BiOI < BiOI < Ti(50 mol%)–BiOI. Upon the addition of scavengers for $^{\bullet}O_2^-$ and h^+, the dye degradation (or the shift in peak position) was dramatically suppressed. The dye with the scavenger of $^{\bullet}O_2^-$ showed some degradation, but no change in the absorption peak position. This indicates that other active species such as h^+ dissociate the dye without forming a secondary product (discussed later). However, the scavenger for the $^{\bullet}OH$ radical showed no suppression and the same degradation rate as the dye solution without a scavenger. These results indicate that the $^{\bullet}O_2^-$ and h^+ species are formed during visible light irradiation, and that they play important roles in dye degradation, which agrees well with the available literature.[2,3,5,14,19,22] Li *et al.* also found that the $^{\bullet}O_2^-$ and h^+ species play major roles in degradation, but the $^{\bullet}OH$ radical showed no effect on the degradation of phenol with a $BiOI/ZnSn(OH)_6$ catalyst.[5] For the BiOI and Ti–BiOI catalysts, the h^+ appears to be more important than $^{\bullet}O_2^-$. Ye *et al.* reported a similar result for BiOI.[3] Furthermore, they found that $^{\bullet}O_2^-$ became

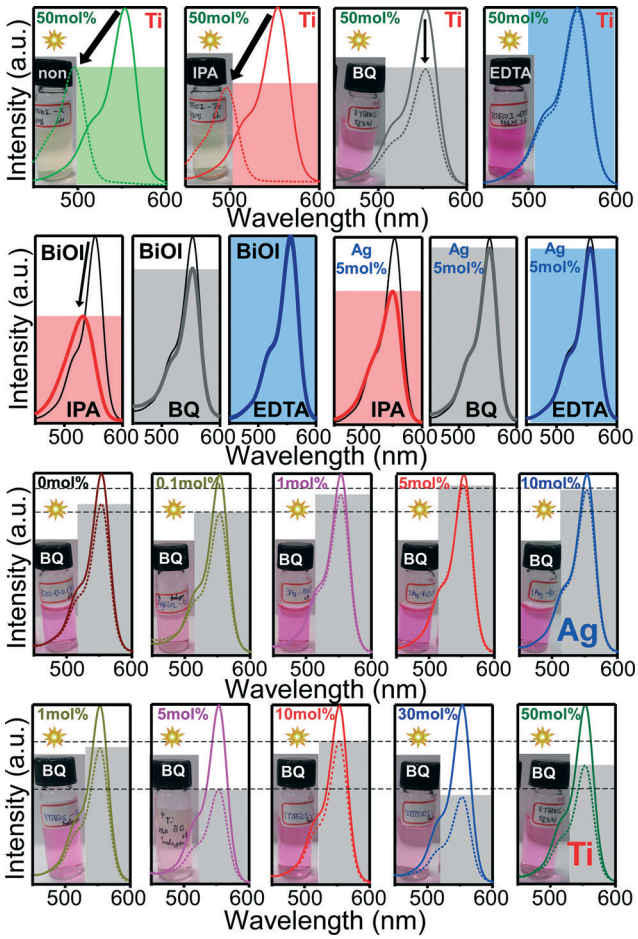

Fig. 11 The photocatalytic degradation (top two lines) of RhB with BiOI, Ag(5 mol%)–BiOI and Ti(50 mol%)–BiOI in the absence and presence of scavengers (IPA, BQ and EDTA) under visible light irradiation for 6 hours. The photocatalytic degradation (bottom two lines) of RhB over Ag–BiOI and Ti–BiOI with different Ag and Ti-loaded BiOI in the presence of BQ under visible light irradiation for 6 hours.

more important than the h^+ species for Pt–BiOI.[3] Similarly, in the present study, the $^{\bullet}O_2^-$ and h^+ species showed comparable activities for Ag–BiOI, which were attributed to an enhanced electron transfer followed by the generation of $^{\bullet}O_2^-$.[29,30] Liu *et al.* used Ag/BiOI composites to degrade acid orange II, MO and RhB under visible-light irradiation and found a higher photocatalytic activity than BiOI.[29] They explained that the electrons in the CB of BiOI accumulated on the surface of Ag and were more easily transferred to the adsorbed surface oxygen to form active $^{\bullet}O_2^-$. Since a partial degradation of RhB was found with the $^{\bullet}O_2^-$ scavenger, we further examined the effect of BQ over the catalyst with different Ag and Ti-loadings (Fig. 11). The dye degradation was found to be dependent on the Ag or Ti-content. The BiOI with higher loadings of Ag (1, 5 and 10 mol%) showed a poor degradation, compared with undoped and 0.1 mol% Ag-doped BiOI. On the other hand, the Ti–BiOI catalysts showed a better photodegradation performance as discussed in Fig. 10 for RhB under visible light irradiation.

To confirm that $^{\bullet}OH$ had no effect on the dye degradation, we employed photoluminescence spectroscopy using terephthalic acid.[20,22,27,51] When $^{\bullet}OH$ radicals are formed in response to visible light irradiation they react with terephthalic acid to form luminescent (λ_{em} = 425 nm) 2-hydroxyterephthalic acid. We observed no significant emission signal (Fig. S7, ESI†) at 425 nm for the BiOI, Ag(10%)–BiOI or Ti(5%)–BiOI catalysts after visible light irradiation or UV irradiation for 6 hours, confirming that no significant $^{\bullet}OH$ radical was produced during the photoirradiation, and that it was not involved in the photodegradation reaction. For the Bi_2S_3/BiOI catalyst under visible light irradiation, Cao *et al.* observed a photoluminescence peak at 425 nm, which was attributed to the formation of $^{\bullet}OH$ radicals.[27] However, they found that the $^{\bullet}OH$ radical effect was not as strong as that of the $^{\bullet}O_2^-$ and h^+ species for the degradation of MO.

We further examined the photodegradation of BiOI with different amounts of Ag and Ti-loadings without adding any scavengers. Fig. 12 shows that 0.1 mol% Ag–BiOI is the most efficient catalyst for RhB dye degradation and there is a shift in the absorbance position of the dye solution. However, BiOI with 1, 5 and 10 mol% Ag showed poor degradation and smaller shift in the peak position. This indicates that RhB is poorly degraded when the amount of Ag was loaded above 1 mol%. Lu *et al.* prepared a Ag-modified (0.2–2.0 wt%) BiOBr catalyst and tested the photodegradation of RhB under visible light.[65] They found a similar catalytic behaviour for pure BiOBr with a higher catalytic activity than that of Ag-modified BiOBr. They attributed the poor performance of the Ag-modified BiOBr to the formation of Ag_2O. However, Kong *et al.* found an enhanced photocatalytic

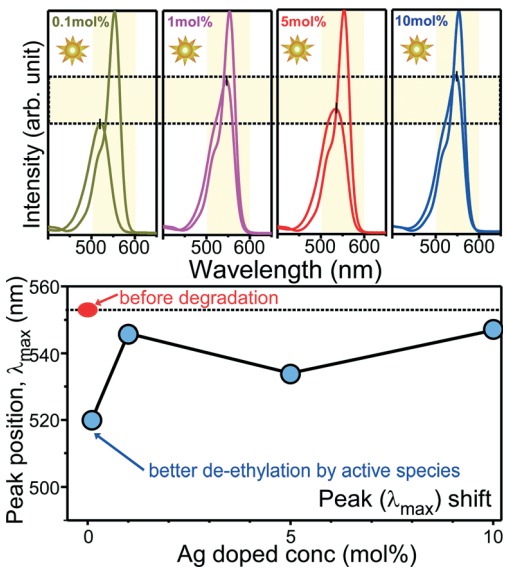

Fig. 12 The photocatalytic degradation (and the change in peak position) of RhB over BiOI with Ag-loading under visible light irradiation for 6 hours. The UV-visible absorption peaks were normalized before photoirradiation.

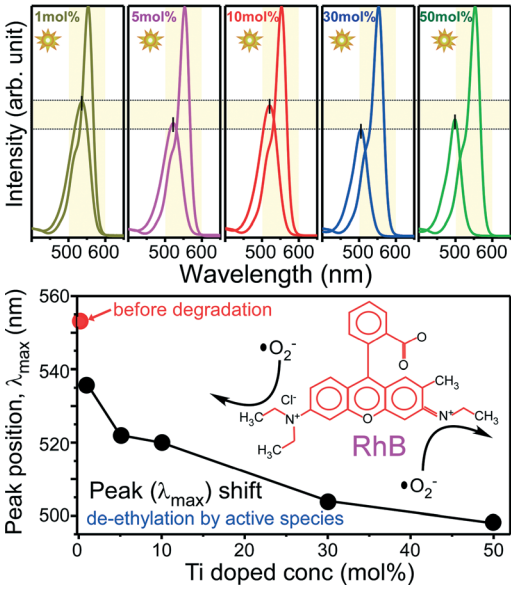

Fig. 13 The photocatalytic degradation (and the change in peak position) of RhB over BiOI with different Ti-loadings under visible light irradiation for 6 hours. The UV-Vis. absorption peaks were normalized before photoirradiation.

performance with loadings below 0.5 wt% AgBr, and a poor performance above 1.0 wt% AgBr, compared with pure BiOBr.[66]

For the Ti-loaded BiOI (Fig. 13), the UV-visible absorption intensity showed no linear relationship with the Ti-amount. However, the blue shift in the peak position was linearly increased with the increasing the Ti-amount. This indicates that $^{\bullet}O_2^-$ radical became more important as the Ti-amount was increased in BiOI. The $^{\bullet}O_2^-$ radical may attack the *N*-ethyl group of RhB (as shown in the inset of Fig. 13) to initially form secondary products, which results in the blue-shift in the absorption position.[67]

Based on the aforementioned results, the following photodegradation mechanism was proposed[27,43] under visible ($\lambda > 420$ nm) light irradiation for BiOI and doped BiOI (Fig. 14).

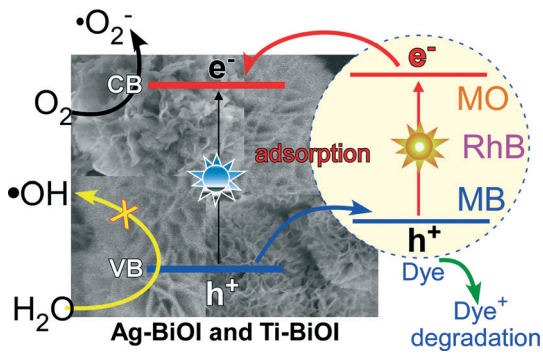

Fig. 14 The photocatalytic degradation mechanism of a dye over the catalysts.

$$\text{dye} + \text{visible light} \rightarrow \text{dye}\,(e_{CB}^- + h_{VB}^+) \quad (1)$$

$$\text{adsorbed dye}\,(e_{CB}^- + h_{VB}^+) + \text{BiOI} \rightarrow \text{BiOI}\,(e_{CB}^-) + \text{dye}\,(h_{VB}^+) \quad (2)$$

$$\text{BiOI} + \text{UV and visible light} \rightarrow \text{BiOI}\,(e_{CB}^- + h_{VB}^+) \quad (3)$$

$$\text{BiOI}\,(e_{CB}^-) + \text{adsorbed } O_2(\text{or surface O}) \rightarrow {}^{\bullet}O_2^-(\text{or } {}^{\bullet}O^-) + \text{BiOI} \quad (4)$$

$$H_2O \rightarrow H^+ + OH^- \quad (5)$$

$${}^{\bullet}O_2^-(\text{or } {}^{\bullet}O^-) + H^+ \rightarrow {}^{\bullet}O_2H\ (\text{or } {}^{\bullet}OH) \quad (6)$$

$$OH^- + \text{BiOI}\,(h_{VB}^+) \rightarrow {}^{\bullet}OH \quad (7)$$

$$H_2O + \text{BiOI}\,(h_{VB}^+) \rightarrow H^+ + {}^{\bullet}OH \quad (8)$$

$${}^{\bullet}O_2^-, h^+ \text{or } {}^{\bullet}OH + \text{adsorbed dye/dye}^+ \rightarrow \text{degradation products} \quad (9)$$

When a dye absorbs visible light, an electron (e^-) and a hole (h^+) are created in the conduction and valence bands (CB and VB), respectively. In a dye sensitized mechanism,[22,61,62] the electron in the CB transfers to the CB of the catalyst before being recombined with a hole (Fig. 14). The transfer rate is determined by good interfacial wavefunction mixing (and good adsorption) between the dye and the catalyst. Based on the UV-Vis absorption spectra (Fig. 6), the catalyst could directly absorb UV or visible light to create e^- and h^+ in the CB and VB, respectively. The electron in the CB of the catalyst is captured by the adsorbed molecular (or atomic) oxygen to form $^{\bullet}O_2^-$ (or $^{\bullet}O^-$) radicals, which degrade the adsorbed dye.[30] As shown in Fig. 11, the $^{\bullet}O_2^-$ scavenger suppressed dye degradation. Additionally, oxygen vacancies have been shown to play active roles in dye degradation.[68] The electron in the energy state of the oxygen vacancy was trapped by the surface oxygen to create active $^{\bullet}O_2^-$, and the $^{\bullet}O_2^-$ radical may have proceeded to form active $^{\bullet}OH$ radicals. The adsorbed OH^- species may also capture the hole in the VB of BiOI to form $^{\bullet}OH$ radicals.[51,59] However, the $^{\bullet}OH$ radical was not involved in the dye degradation because there was no $^{\bullet}OH$ scavenger effect and no PL emission of 2-hydroxyterephthalic acid. The h_{VB}^+ in the catalyst or in the dye acts as an active species to finally degrade the dye,[47] as confirmed by the hole scavenger test. Consequently, the O_2^- and h^+ species primarily degrade the dye, which is consistent with the available literature.[2,3,5]

Finally, to emphasize the originality and new results of the present study, we summarized the literatures using similar catalysts in Table 3. The AgI/BiOI (or Ag/BiOI) catalysts were commonly synthesized as follows: BiOI was first synthesized and then dispersed in an $AgNO_3$ solution.[1,2,4,10,11,29,30] AgI was formed at the interface by an ion exchange reaction. However, we mixed bismuth nitrate, $AgNO_3$ (or Ti isopropoxide) and KI together in EG, and treated at 120 °C for 12 hours. Cheng *et al.* synthesized AgI/BiOI using a similar method, but used a mixed EtOH/H_2O solvent, and a thermal

Table 3 A summary of the literatures using similar catalyst systems

Catalysts	Experimental conditions	Test systems and performances
AgI(16–400 nm)/BiOI[1]	BiOI in $AgNO_3$ EG solution, ion exchange	2,4-Dichlorophenol, under Vis., enhanced
AgI(15.7, 28.2, 35.2, 47.0, 70.4%)/BiOI microspheres[2]	BiOI in $AgNO_3$ aq. solution, ion exchange	RhB and phenolunder Vis., enhanced, max at 70.4% AgI
AgI(10, 40, 60%)/BiOI[4]	BiOI in $AgNO_3$ aq. solution	MO, RhB, MB under Vis., enhanced (best at 40%, and MB > RhB > MO)
AgI(0–100%)/BiOI[47]	Bi nitrate + $AgNO_3$ + KI in EtOH/H_2O (85 °C, 2 hours)	MO and phenol enhanced compared with BiOI, best at 20% AgI
Ag/BiOI(0.3, 0.6, 0.9%)[29]	BiOI in $AgNO_3$ sol. and UV photoirradiation	Acid orange II, MO, RhB under Vis., enhanced, best at 0.6%
Ag/BiOI(1.1, 2.1, 4.5, 8.0%)[30]	BiOI in $AgNO_3$ sol. and photoirradiation	*E. coli* 8099, under Vis., enhanced, best at 4.5%
Ag/AgI/BiOI[10]	BiOI in $AgNO_3$ aq. sol., photoirradiation	MB and *o*-nitrophenol, under Vis., enhanced
Ag/AgI/BiOI[11]	BiOI in $AgNO_3$ EtOH/H_2O sol., photoirradiation	MO, under Vis., enhanced
TiO_2(0–100%)/BiOI[31]	Bi nitrate + tetrabutyl titanate aq. sol.: reverse microemulsions.	MO, enhanced, best at 25%, under Vis.
BiOI-coated on TiO_2 nanotube wall[35]	Impregnating-hydroxylation method using BiI_3	MO, under Vis., enhanced,
TiO_2(1–2%, 50%)/BiOI[36]	Bi nitrate (EG) + $AgNO_3$ (EG) + TiO_2 (H_2O)	Phenol under Vis., best at 25%
Echinoid-like BiOI, AgI/BiOI and Ti–BiOI microsphere (*this work*)	Bi nitrate + $AgNO_3$ (or Ti isopropoxide) + KI in EG (120 °C, 12 hours)	MO, RhB, MB under UV and Vis.

treatment at 85 °C for 2 hours.[47] They examined the photodegradation of MO and phenol under visible light irradiation, and found an enhanced catalytic performance upon Ag-loading, which is consistent without result for MO. However, we further examined RhB and MB under UV light as well as visible light, and the new results were discussed earlier. There was no report on the photocatalytic study performed under UV light with the loaded BiOI. The Ti–BiOI catalyst was synthesized differently in the present work, and carefully tested for MO, RhB and MB which have different molecular structures and UV-visible absorption bands. The Ti-loading enhances the catalytic performance for MO under UV and visible light. For RhB, the Ti-loading showed an enhanced effect under visible light, but poor performance under UV light, compared with un-loaded BiOI.

4. Conclusion

Echinoid flower-like BiOI with various concentrations of Ag (0.1, 1.0, 5.0, 10.0 mol%) and Ti (1.0, 5.0, 10.0, 30.0, 50.0 mol%) was successfully synthesized in an ethylene glycol environment and their fundamental properties were examined by SEM, XRD, UV-visible absorption, Raman, FT-IR, photoluminescence and BET surface area measurements. The adsorption and photocatalytic performances were demonstrated for MO, RhB and MB. The adsorption performance was mainly related to the nature of the dye and the catalyst surface structure, not the surface area.

New important findings of the present study are as follows:

1) MB was commonly the most efficiently adsorbed by the catalysts, while none of the catalysts adsorbed MO well. Overall, the adsorption was found to be in the order of MO $\ll$ RhB $<$ MB, which was attributed to electrostatic interactions between the dye and the catalyst surface.

2) MO was efficiently photodegraded by the catalysts under UV and visible light in the order of BiOI $<$ Ag–BiOI $<$ Ti–BiOI. For RhB, BiOI was an efficient photocatalyst under UV irradiation, while Ag and Ti-loaded BiOI showed a poor photocatalytic activity. Under visible light irradiation, the catalysts showed a good catalytic activity with an order of Ag–BiOI $<$ BiOI $<$ Ti–BiOI. MB showed poor photodegradation with the catalysts under both UV and visible light irradiation.

3) A dye sensitized mechanism was proposed in which light absorption by the dye followed by a charge transfer from the dye to the catalyst is involved. The active species of $^{\bullet}O_2^-$ and h^+ (more active) play important roles in the photocatalytic process. It was found that the $^{\bullet}O_2^-$ species initially create secondary dissociation products, while the h^+ species showed a total dissociation without forming any secondary product. The photocatalytic activity was understood by various factors such as surface area, crystallinity, good interfacial wavefunction mixing (or the well-aligned energy level for change transfer), and the relative role of active species.

The present study provides a new insight that can aid in the selection of an appropriate adsorbent/catalyst for pollutant removal by explaining the adsorption and photodegradation mechanism of MO, RhB and MB with BiOI and Ag and Ti–BiOI catalysts under UV and visible light irradiation.

Acknowledgements

This work was financially supported by the India-Korea joint project, the National Research Foundation of Korea (NRF) grant funded by the Korean government (MEST) (NRF-2012-0006296), and the Department of Science and Technology, New Delhi through the Indo-Korea/P-02 grant.

References

1 H. Cheng, W. Wang, B. Huang, Z. Wang, J. Zhan, X. Qin, X. Zhang and Y. Dai, *J. Mater. Chem. A*, 2013, **1**, 7131–7136.
2 L. Chen, D. Jiang, T. He, Z. Wu and M. Chen, *CrystEngComm*, 2013, **15**, 7556–7563.
3 L. Ye, X. Liu, Q. Zhao, H. Xie and L. Zan, *J. Mater. Chem. A*, 2013, **1**, 8978–8983.
4 Y. Lv, H. Liu, W. Zhang, S. Ran, F. Chi, B. Yang and A. Xia, *J. Environ. Chem. Eng.*, 2013, **1**, 526–533.
5 H. Li, Y. Cui, W. Hong and B. Xu, *Chem. Eng. J.*, 2013, **228**, 1110–1120.
6 H. Li, Y. Cui and W. Hong, *Appl. Surf. Sci.*, 2013, **264**, 581–588.
7 D. K. Ma, S. M. Zhou, X. Hu, Q. R. Jiang and S. M. Huang, *Mater. Chem. Phys.*, 2013, **140**, 11–15.
8 X. Qin, H. Cheng, W. Wang, B. Huang, X. Zhang and Y. Dai, *Mater. Lett.*, 2013, **100**, 285–288.
9 J. Cao, C. Zhou, H. Lin, B. Xu and S. Chen, *Mater. Lett.*, 2013, **109**, 74–77.
10 T. Li, S. Luo and L. Yang, *Mater. Lett.*, 2013, **109**, 247–252.
11 J. Cao, Y. Zhao, H. Lin, B. Xu and S. Chen, *J. Solid State Chem.*, 2013, **206**, 38–44.
12 H. Li, Q. Jia, Y. Cui and S. Fan, *Mater. Lett.*, 2013, **107**, 262–264.
13 J. Cao, B. Xu, H. Lin and S. Chen, *Chem. Eng. J.*, 2013, **228**, 482–488.
14 L. Ye, J. Chen, L. Tian, J. Liu, T. Peng, K. Deng and L. Zan, *Appl. Catal., B*, 2013, **130–131**, 1–7.
15 Y. Lei, G. Wang, P. Guo and H. Song, *Appl. Surf. Sci.*, 2013, **279**, 374–379.
16 Y. Wu, Z. Zhou, Y. Tuo, Y. Huang and S. Shen, *Mater. Lett.*, 2013, **111**, 43–46.
17 G. Li, F. Qin, R. Wang, S. Xiao, H. Sun and R. Chen, *J. Colloid Interface Sci.*, 2013, **409**, 43–51.
18 Z. Cui, M. Si, Z. Zheng, L. Mi, W. Fa and H. Jia, *Catal. Commun.*, 2013, **42**, 121–124.
19 C. Chang, L. Zhu, Y. Fu and X. Chu, *Chem. Eng. J.*, 2013, **233**, 305–314.
20 K. H. Reddy, S. Martha and K. M. Parida, *Inorg. Chem.*, 2013, **52**, 6390–6401.
21 M. Su, C. He, L. Zhu, Z. Sun, C. Shan, Q. Zhang, D. Shu, R. Qiu and Y. Xiong, *J. Hazard. Mater.*, 2012, **229–230**, 72–82.
22 J. Cao, B. Xu, H. Lin, B. Luo and S. Chen, *Chem. Eng. J.*, 2012, **185–186**, 91–99.
23 R. Hao, X. Xiao, X. Zuo, J. Nan and W. Zhang, *J. Hazard. Mater.*, 2012, **209–210**, 137–145.
24 F. Dong, Y. Sun, M. Fu, Z. Wu and S. C. Lee, *J. Hazard. Mater.*, 2012, **219–220**, 26–24.
25 K. Ren, K. Zhang, J. Liu, H. Luo, Y. Huang and X. Yu, *CrystEngComm*, 2012, **14**, 4384–4390.
26 X. Xiao, R. Hao, M. Liang, X. Zuo, J. Nan, L. Li and W. Zhang, *J. Hazard. Mater.*, 2012, **233–234**, 122–130.
27 J. Cao, B. Xu, H. Lin, B. Luo and S. Chen, *Dalton Trans.*, 2012, **41**, 11482–11490.
28 L. Chen, S. F. Yin, S. L. Luo, R. Huang, Q. Zhang, T. Hong and P. C. T. Au, *Ind. Eng. Chem. Res.*, 2012, **51**, 6760–6768.
29 H. Liu, W. Cao, Y. Su, Y. Wang and X. Wang, *Appl. Catal., B*, 2012, **111–112**, 271–279.
30 L. Zhu, C. He, Y. Huang, Z. Chen, D. Xia, M. Su, Y. Xiong, S. Li and D. Shu, *Sep. Purif. Technol.*, 2012, **91**, 59–66.
31 Z. Liu, X. Xu, J. Fang, X. Zhu, J. Chu and B. Li, *Appl. Surf. Sci.*, 2012, **258**, 3771–3778.
32 X. Shi, X. Chen, X. Chen, S. Zhou and S. Lou, *Mater. Lett.*, 2012, **68**, 296–299.
33 N. T. Hahn, S. Hoang, J. L. Self and C. B. Mullins, *ACS Nano*, 2012, **6**, 7712–7722.
34 L. Song, S. Zhang and Q. Wei, *Ind. Eng. Chem. Res.*, 2012, **51**, 1193–1197.
35 G. Dai, J. Yu and G. Liu, *J. Phys. Chem. C*, 2011, **115**, 7339–7346.
36 Y. Li, J. Wang, B. Liu, L. Dang, H. Yao and Z. Li, *Chem. Phys. Lett.*, 2011, **508**, 102–106.
37 J. Cao, B. Xu, B. Luo, H. Lin and S. Chen, *Catal. Commun.*, 2011, **13**, 63–68.
38 Y. Li, J. S. Wang, H. C. Yao, L. Y. Dang and Z. J. Li, *Catal. Commun.*, 2011, **12**, 660–664.
39 M. Liu, L. Zhang, K. Wang and Z. Zheng, *CrystEngComm*, 2011, **13**, 5460–5466.
40 J. Jiang, X. Zhang, P. Sun and L. Zhang, *J. Phys. Chem. C*, 2011, **115**, 20555–20564.
41 T. B. Li, G. Chen, C. Zhou, Z. Y. Shen, R. C. Jin and J. X. Sun, *Dalton Trans.*, 2011, **40**, 6751–6758.
42 Z. Jia, F. Wang, F. Xin and B. Zhang, *Ind. Eng. Chem. Res.*, 2011, **50**, 6688–6694.
43 Y. Li, J. Wang, H. Yao, L. Dang and Z. Li, *J. Mol. Catal. A: Chem.*, 2011, **334**, 116–122.
44 Y. Wang, K. Deng and L. Zhang, *J. Phys. Chem. C*, 2011, **115**, 14300–14308.
45 L. Ye, L. Tian, T. Peng and L. Zan, *J. Mater. Chem.*, 2011, **21**, 12479–12484.
46 C. Yu, J. C. Yu, C. Fan, H. Wen and S. Hu, *Mater. Sci. Eng., B*, 2010, **166**, 213–219.
47 H. Cheng, B. Huang, Y. Dai, X. Qin and X. Zhang, *Langmuir*, 2010, **26**, 6618–6624.
48 Y. Chen, D. Li, X. Wang, L. Wu, X. Wang and X. Fu, *New J. Chem.*, 2005, **29**, 1514–1519.
49 M. Yin, Z. Li, J. Kou and Z. Zou, *Environ. Sci. Technol.*, 2009, **43**, 8361–8366.
50 J. Xu, W. Meng, Y. Zhang, L. Li and C. Guo, *Appl. Catal., B*, 2011, **107**, 355–362.
51 J. Xu, L. Li, C. Guo, Y. Zhang and W. Meng, *Appl. Catal., B*, 2013, **130–131**, 285–292.
52 G. Jiang, X. Wang, Z. Wei, X. Li, X. Xi, R. Hu, B. Tang, R. Wang, S. Wang, T. Wang and W. Chen, *J. Mater. Chem. A*, 2013, **1**, 2406–2410.
53 L. P. Zhu, G. H. Liao, N. C. Bing, L. L. Wang, Y. Yang and H. Y. Xie, *CrystEngComm*, 2010, **12**, 3791–3796.
54 X.-X. Wei, H. Cui, S. Guo, L. Zhao and W. Li, *J. Hazard. Mater.*, 2013, **263**, 650–658.

55 Y. Li, Y. Liu, J. Wang, E. Uchaker, Q. Zhang, S. Sun, Y. Huang, J. Li and G. Cao, *J. Mater. Chem. A*, 2013, **1**, 7949–7956.
56 X. Chang, J. Huang, C. Cheng, Q. Sui, W. Sha, G. Ji, S. Deng and G. Yu, *Catal. Commun.*, 2010, **11**, 460–464.
57 J. Xia, S. Yin, H. Li, H. Xu, L. Xua and Q. Zhang, *Colloids Surf., A*, 2011, **387**, 23–28.
58 D. Zhang, M. Wen, B. Jiang, G. Li and J. C. Yu, *J. Hazard. Mater.*, 2012, **211–212**, 104–111.
59 D. Zhang, J. Li, Q. Wang and Q. Wu, *J. Mater. Chem. A*, 2013, **1**, 8622–8629.
60 Y. Lei, C. Zhang, H. Lei and J. Huo, *J. Colloid Interface Sci.*, 2013, **406**, 178–185.
61 B. Subash, B. Krishnakumar, M. Swaminathan and M. Shanthi, *Langmuir*, 2013, **29**, 939–949.
62 Y. F. Fang, W. H. Ma, Y. P. Huang and G. W. Cheng, *Chem.–Eur. J.*, 2013, **19**, 3224–3229.
63 N. Roy, Y. Sohn and D. Pradhan, *ACS Nano*, 2013, **7**, 2532–2540.
64 G. Jiang, R. Wang, X. Wang, X. Xi, R. Hu, Y. Zhou, S. Wang, T. Wang and W. Chen, *ACS Appl. Mater. Interfaces*, 2012, **4**, 4440–4444.
65 L. Lu, L. Kong, Z. Jiang, H. H.-C. Lai, T. Xiao and P. P. Edwards, *Catal. Lett.*, 2012, **142**, 771–778.
66 L. Kong, Z. Jiang, H. H. Lai, R. J. Nicholls, T. Xiao, M. O. Jones and P. P. Edwards, *J. Catal.*, 2012, **293**, 116–125.
67 Z. Jia, F. Wang, F. Xin and B. Zhang, *Ind. Eng. Chem. Res.*, 2011, **50**, 6688–6694.
68 L. Ye, K. Deng, F. Xu, L. Tian, T. Peng and L. Zan, *Phys. Chem. Chem. Phys.*, 2012, **14**, 82–85.